

## Article

# Research on Temperature Rise of Type IV Composite Hydrogen Storage Cylinders in Hydrogen Fast-Filling Process

Jiepu Li <sup>1,2</sup> , Junhao Liu <sup>1,2,3</sup>, Baodi Zhao <sup>1,2</sup>, Dongyu Wang <sup>4,\*</sup>, Shufen Guo <sup>4</sup>, Jitian Song <sup>3</sup> and Xiang Li <sup>1,2,\*</sup><sup>1</sup> China Special Equipment Inspection and Research Institute, Beijing 100029, China<sup>2</sup> Key Laboratory of Safety of Hydrogen Energy Storage and Transportation Equipment for State Market Regulation, Beijing 100029, China<sup>3</sup> College of Mechanical Engineering, Tianjin University of Science and Technology, Tianjin 300222, China<sup>4</sup> FTXT Energy Technology Co., Ltd., Shanghai 201804, China

\* Correspondence: wangdongyu@ftxt-e.com (D.W.); lixiang@csei.org.cn (X.L.)

**Abstract:** The internal pressure and temperature of type IV on-board hydrogen storage cylinders constantly change during the hydrogen fast-filling process. In this work, a 2D axisymmetric computational fluid dynamics (CFD) model is established to study the temperature rise of hydrogen storage cylinders during the fast-filling process. The hydrogen filling rate, ambient temperature, volume, and hydrogen inlet temperature were investigated to evaluate their effects on temperature rise inside the cylinders. The effects of the inlet pressure rise and pre-cooling patterns on the temperature rise of large-volume type IV hydrogen storage cylinders are analyzed, and the optimal filling strategy is determined. The research results show that a greater filling rate causes a higher hydrogen temperature rise at the end. The ambient temperature increases linearly with the maximum hydrogen temperature and decreases linearly with the state of charge (SOC). As the volume increases, the temperature rise of the cylinder increases. Reducing the inlet hydrogen temperature helps control the temperature rise, and the hydrogen inlet pre-cooling temperature required for large-volume cylinders is lower. If the filling time remains unchanged, a high pressure rise rate should be avoided, and a linear pressure rise pattern is optimal. Reducing the initial cooling energy is key to optimizing the filling strategy.

**Keywords:** hydrogen storage cylinder; temperature rise; fast-filling; numerical simulation



**Citation:** Li, J.; Liu, J.; Zhao, B.; Wang, D.; Guo, S.; Song, J.; Li, X. Research on Temperature Rise of Type IV Composite Hydrogen Storage Cylinders in Hydrogen Fast-Filling Process. *Energies* **2023**, *16*, 2918. <https://doi.org/10.3390/en16062918>

Academic Editor: Lorenzo Ferrari

Received: 13 February 2023

Revised: 17 March 2023

Accepted: 21 March 2023

Published: 22 March 2023



**Copyright:** © 2023 by the authors. Licensee MDPI, Basel, Switzerland. This article is an open access article distributed under the terms and conditions of the Creative Commons Attribution (CC BY) license (<https://creativecommons.org/licenses/by/4.0/>).

## 1. Introduction

With the increasingly significant global greenhouse effect, the goals of peak carbon dioxide emissions and carbon neutrality have been proposed, and countries have accelerated explorations of new energy sources [1–3]. Hydrogen energy is among the most promising secondary energy sources this century due to the advantages of abundant reserves, pollution-free operations, high combustion calorific value, zero emissions, and renewability [4–6]. The main application of hydrogen energy is in the field of transportation; thus, hydrogen fuel cell vehicles (HFCV) have attracted significant attention [7]. The most mature and widely used on-board hydrogen storage method is high-pressure gaseous hydrogen storage, which uses mainly on-board type III and type IV hydrogen storage cylinders with nominal working pressures of 35 or 70 MPa [8,9]. The plastic liner materials of type IV hydrogen storage cylinders use high-density polyethylene (HDPE) or polyamide (PA), along with carbon-fiber-reinforced polymer (CFRP) material as the loading layers [10–12]. Type IV hydrogen storage cylinders have the characteristics of being lightweight, with a high hydrogen storage density and good fatigue performance and have become ubiquitous in research [13].

Hydrogen fuel cell vehicles need to fill cylinders to a higher density within 180–300 s to meet an endurance mileage of 500 km [14,15]. The internal pressure and temperature of hydrogen storage cylinders increase significantly during filling, which is not adiabatic. Due to the compression effect and other factors, the hydrogen temperature increases rapidly,

and the internal heat is transferred to the external environment via conduction [16–18]. As CFRP materials are sensitive to temperature, higher hydrogen temperatures tend to reduce the mechanical properties of the material, which directly impacts the safety of on-board hydrogen storage systems [19]. During the filling process, a greater hydrogen temperature causes a lower hydrogen density and an under-filled state [20]. To ensure the safety of filling processes of on-board hydrogen storage systems, the standard SAE J2601 as formulated by the Society of Automotive Engineers requires that hydrogen storage cylinders meet the following requirements at the end of filling: the maximum temperature should not exceed 358 K, the allowable pressure is 1.25 times the nominal working pressure (NWP), cylinders should not be in an under-/over-filled state, and the state of charge (SOC) of the filling state should be within a reasonable range of 90–100%. For hydrogen storage cylinders with an NWP of 70 Mpa, the hydrogen density when the SOC reaches 100% is 40.2 kg/m<sup>3</sup> [21]. Therefore, we focus on the temperature rise during the filling process of on-board high-pressure hydrogen storage cylinders and determine the appropriate filling strategies.

Lee, T., et al. [22] numerically and experimentally studied the hydrogen filling process in the storage tank of the hydrogen charging station; a Computational Fluid Dynamics model for non-adiabatic real filling of a 50 MPa 343 L stainless steel hydrogen cylinder (type I) was presented, and the experimental results were in good agreement with the simulation results. An accurate formula was used to calculate the final temperature rise by fitting the simulation results, which can achieve effective control of the temperature. Lee et al. [23] established a thermodynamic model on the basis of the hydrogen fast charging process, and the theoretical analysis was used to quantitatively determine the temperature, mass, and filling time in the fast-filling process. The laws of conservation of mass and energy were combined with the equation of real gas state to derive the expression of temperature in the type III hydrogen storage tank. Liu, B., et al. [24] established a 2D axisymmetric model to simulate the filling process of hydrogen storage cylinders with a rated working pressure of 35 MPa and a volume of 150 L; the influence of hydrogen filling at different temperatures on the temperature rise, pressure, and SOC of the high-pressure hydrogen storage cylinder was revealed. Moreover, by subjecting the injected hydrogen to precooling treatment, the temperature rise rate and the maximum temperature rise inside the cylinder could be reduced. Liu et al. [25,26] numerically and experimentally investigated thermal behaviors, such as temperature rise and distributions, inside 35 MPa, 150 L type III hydrogen storage cylinders during refueling. They found that the maximum temperature rise at the interface of the cylinder was in the caudal region and increased with the mass filling rate and ambient temperature. However, it decreased at higher initial pressures. Similar conclusions were obtained from the studies of Hirotsu et al. [27] and Zhao et al. [28]. The above research adopts mainly theoretical analysis, numerical simulation, experimental research, and other methods to analyze the temperature rise of the fast hydrogen filling process of type I and type III cylinders, which has reference significance for the research of type IV. However, because the liner of type IV cylinder is of plastic material with poor thermal conductivity, its temperature rise rules are different from those of type I and type III cylinders.

In the study of the temperature rise of the fast hydrogen filling process of type IV cylinders, Jun Liu et al. [29] used a 2D axisymmetric computational fluid dynamics (CFD) model to simulate the fast-filling and holding processes of 70 MPa hydrogen storage cylinders. Their simulation results showed that the temperature distribution during filling differed for various type III storage cylinders. The greatest temperature was always in the head dome junction region for type IV storage cylinders. Acosta et al. [30,31] used numerical and experimental methods to investigate the fast-filling scenarios for 70 MPa, 29 L type IV hydrogen storage cylinders. Varying rates of pressure rise, adiabatic processes, and cold filling were investigated to evaluate the effects on the maximum hydrogen temperature inside the cylinders. Deng and Xiao et al. [32,33] used the analytic solution of the final hydrogen temperature derived from the hydrogen filling theoretical model to determine

the relationship between the final hydrogen temperature and initial temperature with the inlet and ambient temperatures. Melideo et al. [34] used CFD to investigate fast filling strategies for 70 MPa, 28.9 L type IV hydrogen tanks and their effects on the key parameters. They found that the most convenient filling strategy from a cooling energy perspective is a nearly linear pressure rise and pre-cooling in the second half of the process.

In summary, existing research results have analyzed primarily the temperature rise during fast-filling processes and filling strategies of type I cylinders, type III hydrogen storage cylinders with nominal working pressure below 70 Mpa, or 70 Mpa type IV hydrogen storage cylinders with the volume below 300 L. Few studies have considered the temperature rise and filling strategies of 70 Mpa type IV hydrogen storage cylinders with volumes greater than 300 L. The SAE J2601 and other hydrogen fueling protocols establish the process limits for hydrogen fuel cell vehicles with total volume capacities less than or equal to 300 L. These protocols stipulate that the maximum mass flow rate during fast-filling is 60 g/s with a filling time of 180–300 s. The volume of a 70 Mpa type IV hydrogen storage cylinder for hydrogen fuel cells in heavy-duty trucks is generally larger than 300 L. When the mass flow rate is less than or equal to 60 g/s, the filling of large-volume on-board hydrogen storage systems cannot be completed within 180–300 s. Therefore, it is necessary to further study hydrogen filling for large-volume 70 Mpa type IV hydrogen storage cylinders and optimize the hydrogen pre-cooling strategies and inlet pressure rise patterns of the filling process.

On the basis of the commonly used computational fluid dynamics software Fluent, a CFD model of transient flow is established in this paper, and the temperature rise of 70 Mpa type IV on-board hydrogen storage cylinders during the hydrogen fast-filling process is studied. The accuracy of the CFD model is verified through fast-filling experiments. On the basis of the developed model, the hydrogen filling rate, ambient temperature, volume, and hydrogen inlet temperature are investigated to evaluate the effects on the maximum hydrogen temperature inside the cylinders. Moreover, the effects of the inlet pressure rise patterns and pre-cooling patterns on the temperature rise of large-volume type IV hydrogen storage cylinders are analyzed, and the optimal filling strategy is determined.

## 2. CFD Simulations

Because 70 Mpa type IV hydrogen storage cylinders have an axisymmetric structure, a 2D axisymmetric mathematical model is established without considering the effects of hydrogen buoyancy on the hydrogen flow to reduce the calculation time and ensure the accuracy of temperature rise during the hydrogen filling process.

### 2.1. Assumptions

Considering that the heat transfer mechanism during hydrogen filling is complex, the physical process needs to be simplified. The basic assumptions of the model are as follows:

- (1) Due to the high hydrogen flow rate, it passes through the valve relatively quickly without significant energy exchange. Therefore, this study ignores the energy exchange between hydrogen and the valve.
- (2) The thermal conductivity of the CFRP layer is low, and only a small amount of heat is transferred to the outer wall during hydrogen filling. Thus, the convective heat transfer coefficient of the outer CFRP wall has little impact on the heat transfer characteristics of cylinders [35,36]. The constant convective heat transfer coefficient of the outer wall surface of the CFRP is 6 W/(m<sup>2</sup>·K) [37].
- (3) Since a small amount of heat is transferred to the CFRP layer, its thermal conductivity is considered isotropic. The axial and radial thermal conductivity and specific heat capacity change little during the fast-filling process and can be set as constant values.
- (4) On the basis of experimental data, the cylinder inlet is regarded as a pressure boundary that changes with time. Given that the total hydrogen inlet temperature in the experiments are basically the same, it can be set a constant.

- (5) Since the nitrogen will be used for replacement before hydrogen filling, it will be left to stand until its temperature is basically the same as the ambient temperature. Therefore, it can be considered that the initial hydrogen temperature within the cylinder is the same as the wall temperature before filling begins.
- (6) Due to the high flow rate during the filling process, the buoyancy effect has little impact on the heat transfer characteristics of hydrogen filling compared with forced convection. Therefore, the influence of hydrogen buoyancy on the internal flow field is not considered, and the flow in the cylinders is considered to be axisymmetric flow [38–40].
- (7) Due to the small mechanical deformation during the fast-filling process, its influence on the temperature rise of the cylinders can be ignored. All solid materials in the system are assumed to be rigid bodies without mechanical deformation.

## 2.2. Governing Equations

On the basis of the above assumptions, the 2D axisymmetric CFD calculation models are established, including the heat transfer model, flow model, and hydrogen equation of state. The governing equations are described below. The mass conservation equation is:

$$\frac{\partial \rho}{\partial t} + \frac{\partial}{\partial x}(\rho u) + \frac{\partial}{\partial x}(\rho v) \frac{\rho v}{r} = 0 \quad (1)$$

where  $\rho$  is the density,  $t$  is time,  $u$  denotes the axial velocity,  $v$  denotes the radial velocity,  $x$  denotes the axial distance, and  $r$  denotes the radial distance. The momentum transport in the axisymmetric inertial reference frame is described as:

$$\begin{aligned} \frac{\partial}{\partial t}(\rho u) + \frac{1}{r} \frac{\partial}{\partial x}(r \rho u u) + \frac{1}{r} \frac{\partial}{\partial r}(r \rho v u) = & -\frac{\partial p}{\partial x} + \frac{1}{r} \frac{\partial}{\partial x} \left[ r(\mu + \mu_t) \left( 2 \frac{\partial u}{\partial x} - \frac{2}{3} (\nabla \cdot \vec{v}) \right) \right] \\ & + \frac{1}{r} \frac{\partial}{\partial r} \left[ r(\mu + \mu_t) \left( 2 \frac{\partial u}{\partial r} + \frac{\partial v}{\partial x} \right) \right] \end{aligned} \quad (2)$$

where  $p$  denotes the absolute pressure,  $\mu$  denotes the dynamic viscosity, and  $\mu_t$  denotes the turbulence viscosity. The energy equation for hydrogen in the axisymmetric inertial reference frame is:

$$\frac{\partial}{\partial t}(\rho E) + \frac{\partial}{\partial x}(u(\rho E + p)) = \frac{\partial}{\partial r} \left[ k_{eff} \frac{\partial \tau}{\partial r} + u(\mu + \mu_t) \left( \frac{\partial u}{\partial r} + \frac{\partial v}{\partial x} \right) - \frac{2}{3} u(\mu + \mu_t) \frac{\partial u}{\partial x} \right] \quad (3)$$

where  $k_{eff}$  is the effective thermal conductivity and  $E$  is:

$$E = h - \frac{p}{\rho} + \frac{u^2}{2} \quad (4)$$

where  $h$  denotes the specific enthalpy of hydrogen.

Suryan et al. [41–43] compared different turbulence model performances for refueling compressed hydrogen tanks. They observed that the Realizable  $k$ - $\varepsilon$  model is the most suitable for turbulence in the hydrogen tank filling problem. The turbulence kinetic energy  $k$  and its rate of dissipation  $\varepsilon$  model are obtained from the following transport equations:

$$\frac{\partial}{\partial t}(\rho k) + \frac{\partial}{\partial r}(\rho k u) = \frac{\partial}{\partial r} \left[ \left( \mu + \frac{\mu_t}{\sigma_k} \right) \frac{\partial k}{\partial r} \right] + G_k - \rho \varepsilon - Y_M \quad (5)$$

$$\frac{\partial}{\partial t}(\rho \varepsilon) + \frac{\partial}{\partial r}(\rho \varepsilon u) = \frac{\partial}{\partial r} \left[ \left( \mu + \frac{\mu_t}{\sigma_\varepsilon} \right) \frac{\partial \varepsilon}{\partial r} \right] + \rho C_1 S \varepsilon - \rho C_2 \frac{\varepsilon^2}{k + \sqrt{v \varepsilon}} \quad (6)$$

where  $C_1$  and  $C_2$  are constants ( $C_1 = \max [0.43, \frac{\eta}{\eta+5}]$  and  $C_2 = 1.9$ ), and  $G_k$  denotes the generation of turbulence kinetic energy as the mean velocity gradient as:

$$G_K = -\overline{\rho u'v'} \frac{\partial v}{\partial x} \quad (7)$$

where  $-\overline{\rho u'v'}$  denotes the Reynolds stress tensor,  $u'$  and  $v'$  denote fluctuating quantities, and  $Y_M$  denotes the contribution of the fluctuating dilatation in compressible turbulence to the overall dissipation rate, which is calculated as:

$$Y_M = 2\rho\varepsilon M_t^2 \quad (8)$$

where  $M_t$  is the turbulent Mach number defined as:

$$M_t = \sqrt{\frac{k}{a^2}} \quad (9)$$

where  $a$  is the speed of sound. The turbulent viscosity  $\mu_t$  is described as:

$$\mu_t = \rho C_\mu \frac{k^2}{\varepsilon} \quad (10)$$

The difference between the Realizable  $k$ - $\varepsilon$  model and the standard and RNG models is that  $C_\mu$  is no longer constant but is a function of the mean strain and rotation rates, angular velocity of the system rotation, and the turbulence fields ( $k$  and  $\varepsilon$ ). The results of Sommer et al. [44] show that wall Prandtl constants of 0.3–0.5 for the boundary layer can better predict the fully developed turbulent flow. Therefore, the wall and energy Prandtl constants are taken as 0.5.

The equations for the turbulence model need to be closed with the hydrogen equation of state. The National Institute of Standards and Technology (NIST) Thermodynamics and Transport Properties of Refrigerant and Refrigerant Mixture Database Version 7.0 (REFPROP v7.0) are used in this study. The NIST equation is more accurate than other state equations and is suitable for unsteady heat transfer when the temperature boundary conditions change over time, as when filling hydrogen storage cylinders [45].

### 2.3. Geometric Model and Mesh

Two structures of hydrogen storage cylinders are simulated: Cylinder A (type IV, NWP of 70 MPa, and volume of 24 L) and Cylinder B (type IV, NWP of 70 MPa, and volume of 367 L). The structural parameters of the cylinders are shown in Table 1.

**Table 1.** Structural parameters of the considered cylinders.

	Cylinder A	Cylinder B
Type	Type IV	Type IV
Volume/L	24	367
NWP/MPa	70	70
Diameter, $D_i$ /mm	203	500
Total length, $L$ /mm	918	2100
Maximum storage quality, $m$ /kg	0.97	14.8
Inlet diameter, $D_{in}$ /mm	3	5
Plastic liner thickness, $T_1$ /mm	3	5
CFRP layer thickness, $T_2$ /mm	20	40
Application	HFCV passenger car	HFCV heavy-duty truck

The model is split into two computational domains. The first is the fluid domain within the cylinder, and the second is the plastic liner, CFRP layer, boss, and valve domain. The axial thickness of the plastic liner and CFRP layer is uniform. The boss, end plug, and valve are simplified as a single structure with a geometry and computational grid, as shown in Figure 1. The fluid domain uses an unstructured triangle mesh type, which is locally dense at the intake nozzle (highest hydrogen velocity), the inlet jet influence zone

(large temperature gradient), and the boundary layer near the wall. The solid domain is a structured quad mesh for fast and accurate calculations of liquid–solid interfaces and heat transfer in the solid domain. The maximum temperature rise in the first 20 s of filling is taken as the criterion for the grid independence check, as shown in Table 2. When the number of cells is greater than 56,841 and 67,464, respectively, the temperature difference between Cylinder A and Cylinder B is small, so these grid types are selected.

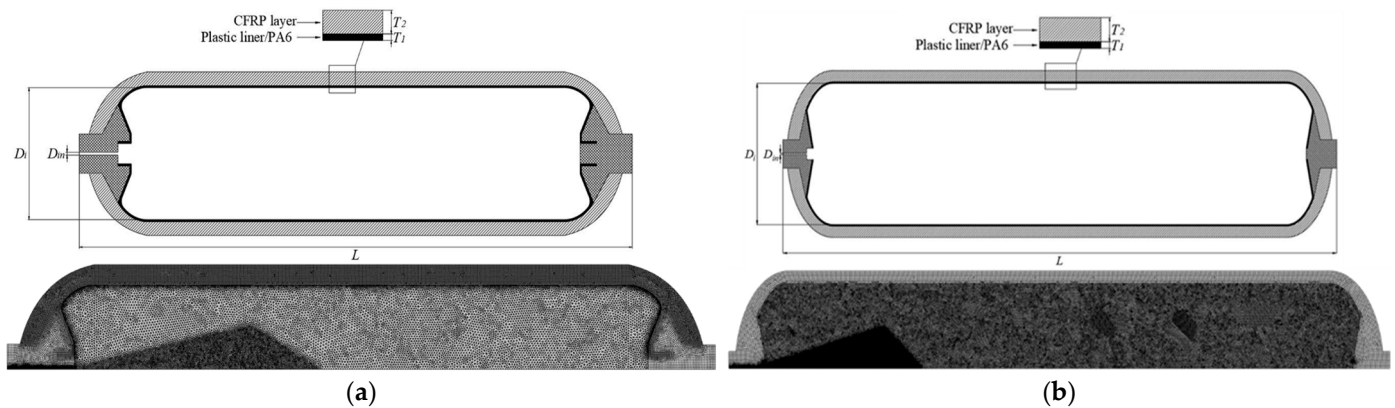


**Figure 1.** Geometric structure and computational grid of the considered cylinders: (a) Cylinder A and (b) Cylinder B.

**Table 2.** Results of the grid independence check.

Cylinder Type	Cells	Hydrogen Max Temperature/K
Cylinder A	27,150	332.8
	56,841	330.7
	75,212	331.2
	125,825	331.3
Cylinder B	59,506	340.5
	67,464	338.0
	176,871	337.9
	307,175	338.2

#### 2.4. Boundary and Solution Conditions

The cylinder filling process is realized primarily by controlling the inlet pressure to adjust the pressure inside the cylinders. The cylinder inlet is regarded as a pressure boundary that changes over time, and a user-defined function (UDF) of Fluent software is used to describe the time-varying total inlet pressure. The interfaces between the plastic liner, hydrogen in the cylinders, and CFRP layer are coupled wall boundaries. The initial pressure for all simulations is 5 MPa. Except for filling simulations of different inlet pressure rise patterns, the pressure inlets have linear patterns. If pre-cooling filling is not considered, the initial temperature of the system and hydrogen inlet temperature are the same as ambient, which is 288 K. The thermal conductivity and specific heat capacity of the plastic liner (PA6) and CFRP layer are measured using pulsed laser heating and differential scanning calorimetry. A summary of the material properties is shown in Table 3.

**Table 3.** Summary of material properties.

Material	Density/kg·m <sup>-3</sup>	Specific Heat/J/(kg·K)	Thermal Conductivity/W/(m·K)
CFRP layer	1220	840	0.48
Plastic liner (PA6)	1000	1788	0.35
Boss (aluminum alloy [18])	2700	902	238

A pressure-based solver is applied to the simulations, and the SIMPLEC algorithm is adopted for the numerical calculations. The transient solution of the physical quantities, such as the pressure and velocity, is determined using an implicit algorithm. The second-order upwind scheme is used for the momentum, turbulent dissipation rate, turbulent kinetic energy, and energy equations. The inner wall of the cylinder is specified as a no-slip boundary condition, and the hydrogen energy equation is coupled with the energy equation of the inner wall. The time step in all simulations is set to 0.0001 s.

### 2.5. CFD Model Validation

To verify the correctness of the CFD model, a hydrogen fast-filling test is performed with a 70 MPa type IV hydrogen storage cylinder in a hydrogen energy laboratory. A flow chart of the experimental system is shown in Figure 2. The hydrogen flows through the 90 MPa high-pressure hydrogen storage container, hydrogen pressure regulating system and pipeline, and finally fills the storage cylinders. The inlet pressure and mass flow rate can be adjusted during the tests. The experimental device and installation position of the cylinders are shown in Figure 3. The cylinder in the tests has the same structure as Cylinder A in the CFD simulations. The test cylinder is placed in a circular pressure cabin, which is placed in a security department filled with nitrogen. The ambient temperature of the pressure cabin and security department are controlled. The research of Jun et al. [46] showed that the maximum temperature rise during fast filling is at the tail in type IV cylinders. Therefore, only one temperature sensor is installed on the end plug of the cylinder to measure the maximum hydrogen temperature rise, and three thermocouples are installed on the outer wall. The temperature sensors are K-type thermocouples with accuracies of  $\pm 1$  K.

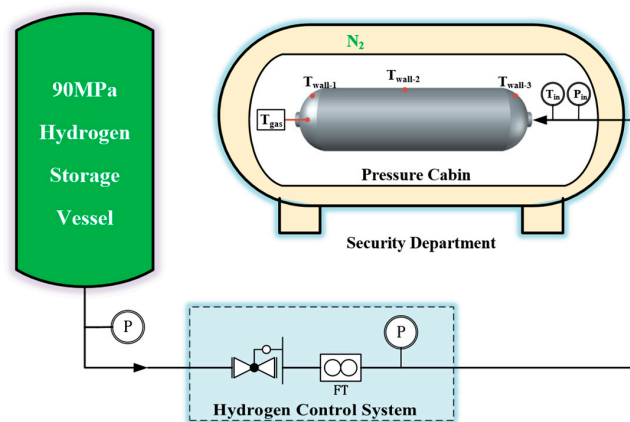


**Figure 2.** Flow chart of the experimental system.

The initial pressure is 7 MPa, the internal temperature of the pressure cabin is 289 K, and the total inlet hydrogen temperature is 293 K. When filling for 71 s, the maximum hydrogen temperature in the cylinder exceeds 358 K, the over-temperature protection function of the test system is activated, and the end pressure is 41.24 MPa. Because a single-stage pressure filling system is adopted, the inlet pressure rises approximately linearly. The inlet pressure curves from the experiments and numerical simulations are shown in Figure 4. A comparison of the temperature rise between the experiments and simulation results is shown in Figure 5 after taking the experimental filling parameters as the boundary conditions in the numerical simulations. The maximum temperature difference between the simulations and experiments is 8 K and occurred in the first 6 s, which may be caused by the approximation of the inlet pressure in Figure 4, as the cylinder pressurization rate was not constant at the beginning of the filling process. At the end of filling, the difference between numerical simulation data and experimental data is 2.1 K, indicating the numerical simulation results agree well with the experimental results, which verifies the accuracy of the CFD model.



Figure 3. Experimental device and installation positions of the cylinders.

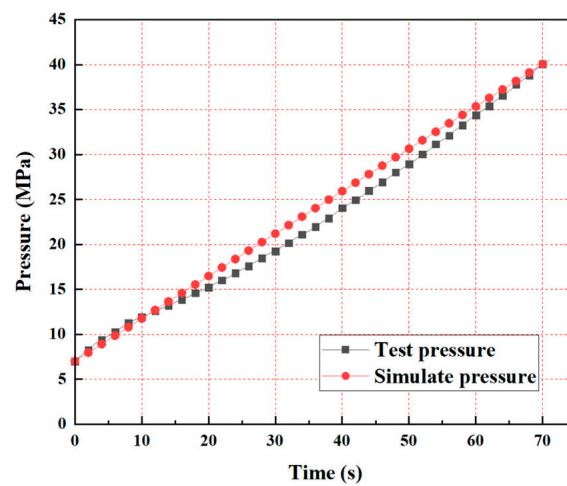


Figure 4. Inlet pressure curves from the experiments and numerical simulations.

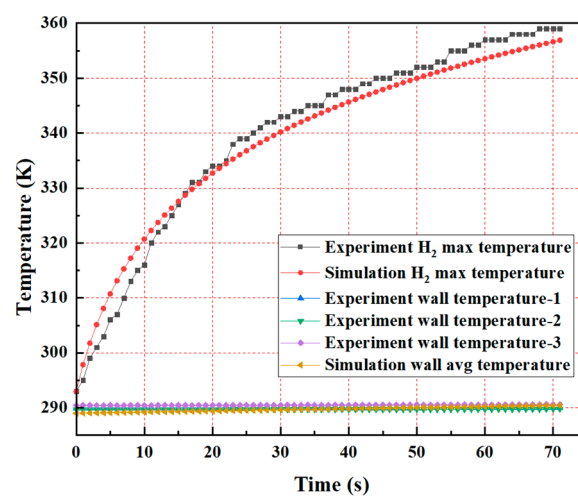


Figure 5. Comparison of the temperature rise between the experiments and simulation results.

### 3. Results

The temperature rises of the 70 MPa type IV hydrogen storage cylinder during the fast-filling process is simulated on the basis of the verified CFD model. The effects of the inlet pressure rise patterns and pre-cooling patterns on the temperature rise of large-volume type IV hydrogen storage cylinders are analyzed, and the optimal filling strategy is determined. The filling parameters for the considered cases are shown in Table 4.

**Table 4.** Filling parameters for the considered cases.

Case	Volume/L	Initial Pressure/MPa	Ending Pressure/MPa	Ambient Temperature/K	Hydrogen Inlet Temperature/K	Filling Rate/MPa/s (Filling Time/s)	Pressure Rise Patterns
1–4	24	5	70	288	288	0.217 (300), 0.361 (180), 0.542 (120), 1.083 (60)	Linear
5–9	24	5	70	258, 273, 288, 298, 313	253	0.361 (180)	Linear
10–11	24, 367	5	70	288	288	0.361 (180)	Linear
12–16	24	5	70	288	233, 253, 263, 273, 288	0.361 (180)	Linear
17–21	367	5	70	288	233, 253, 263, 273, 288	0.361 (180)	Linear
P1–P6	367	5	95% SOC	288	233	198 s	Linear, fast then slow, slow then fast, pressure-holding once, pressure-holding twice, pressure-holding thrice
T1–T4	367	5	95% SOC	288	First 30 s 263 K, then 233 K; First 30 s 273 K, then 233 K; First 30 s 288 K, then 233 K; First 50 s 263 K, then 233 K	198 s	Linear

#### 3.1. Temperature Variations of 70 MPa Hydrogen Fast-Filling Process

The ambient and hydrogen inlet temperatures are both 288 K, the initial pressure is 5 MPa, the end pressure is 70 MPa, and the filling rate is constant at 0.361 MPa/s. The total filling for a 24-L type IV hydrogen storage cylinder is 180 s, and the temperature distributions at 10, 60, 120, and 180 s are shown in Figure 6. As shown in Figure 6, the maximum hydrogen temperatures during filling at different times are near the cylinder tails, which are 313, 345, 354, and 370 K, and the temperature distribution is uneven. This is due to the influence of the inlet hydrogen jet influence zone, the inlet hydrogen jet velocity is higher, the kinetic energy is larger, and the compression effect is not obvious, so the hydrogen temperature is lower. In other regions outside the inlet jet influence zone, due to the low initial pressure in the cylinder, the high-pressure incident hydrogen expands rapidly and mixes with the original hydrogen. After mixing, the incident hydrogen flow rate decreases, and the incident kinetic energy is partially converted into internal energy, resulting in a higher hydrogen temperature. Then, the hydrogen pressure in the cylinder rises, and the hydrogen in the cylinder is compressed to do work, resulting in a compression effect, thereby releasing a large amount of heat. Moreover, the incident hydrogen forms a recirculation flow at the cylinder tails, so that the heat of hydrogen gradually accumulates at the cylinder tails.

The temperature distributions of the plastic liner and CFRP layer are relatively uniform, and the maximum temperature is much lower than the hydrogen temperature in the cylinders. This is because the thermal conductivity of the plastic liner (PA6) is low and the specific heat capacity is high, so the thermal conductivity of the plastic liner (PA6) is poor and the heat storage capacity is strong. The heat of hydrogen is stored mainly in the plastic liner, and only a small amount of heat is transferred to CFRP layer. The temperature at the central axis of the cylinder at the end of filling is shown in Figure 7. As the distance from the inlet increases in the axial direction, the hydrogen temperature increases. Therefore, on the basis of the temperature distribution of the cylinders, it is recommended that the temperature sensor be in the inlet area and away from the jet influence zone to accurately measure the hydrogen temperature in the cylinders during filling.

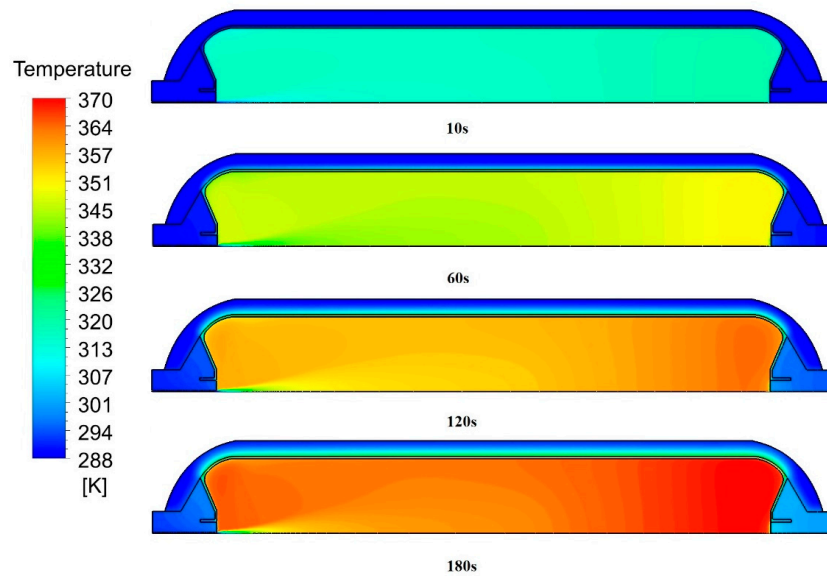


Figure 6. Temperature distributions at 10, 60, 120, and 180 s.

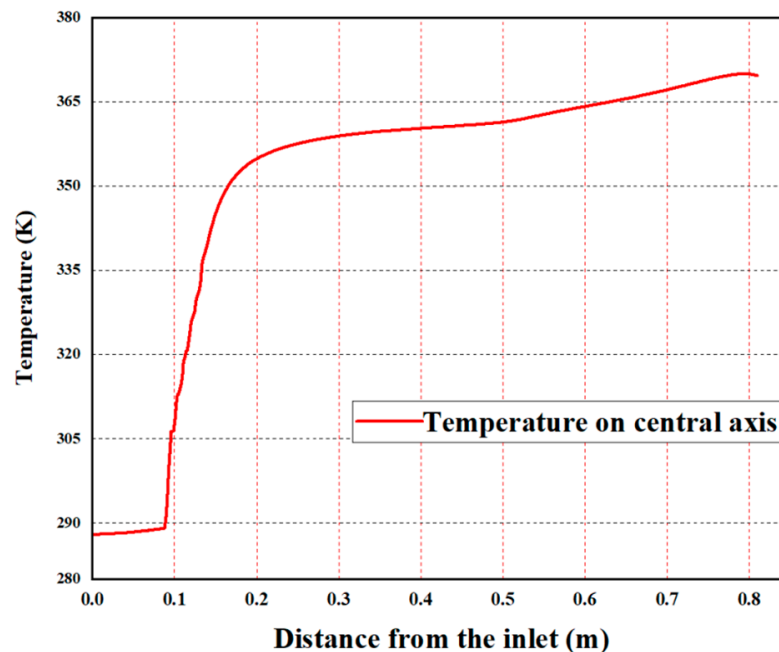


Figure 7. Temperature on the central axis of the cylinder at the end of filling.

The temperature evolutions of hydrogen and solid materials during the 180 s filling process are shown in Figure 8. Due to the obvious compression effect in the initial filling, the hydrogen temperature increases relatively quickly. As the hydrogen pressure increases, the compression effect weakens, and the hydrogen temperature rise is gradually reduced. The thermal conductivity of the plastic liner (PA6) is relatively low, the specific heat capacity is high, and the short-term hydrogen temperature rise is closer to an adiabatic process. When the hydrogen and ambient temperatures are 288 K, the maximum hydrogen temperature in the cylinder reaches 370 K, which exceeds the maximum working temperature of the type IV hydrogen storage cylinders at 358 K. The high temperatures will reduce the mechanical properties of the plastic liner and CFRP layer, which may cause the CFRP layer to peel off and increase the safety risks of the 70 MPa on-board hydrogen storage system.

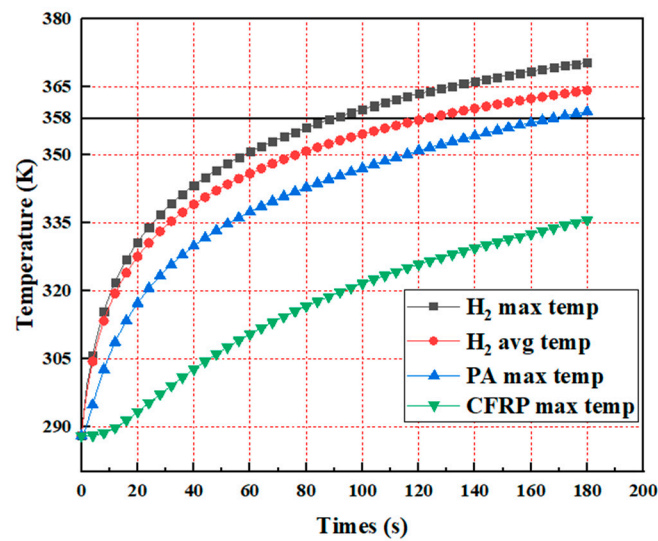


Figure 8. Temperature evolutions of the hydrogen and solid materials.

### 3.2. Effect of Hydrogen Filling Rate

The hydrogen filling rate is usually expressed as the mass flow rate (kg/s) or average pressure rise rate (APRR, MPa/s) [47], where different hydrogen filling rates correspond to various filling times. For Cylinder A (24 L), four hydrogen filling rates of 0.217, 0.361, 0.542, and 1.083 MPa/s are selected, which correspond to filling times of 300, 180, 120, and 60 s, with an inlet hydrogen temperature of 288 K. The other filling parameters are shown as Cases 1–4 in Table 4. The hydrogen temperature rise evolutions at various hydrogen filling rates are shown in Figure 9. As the filling rate increases from 0.217 to 1.083 MPa/s, the hydrogen temperature rise is greater, with maximum values of 357.5, 370, 377.5, and 388 K, respectively. When the system temperature is 288 K, only the temperature rises for the 0.217 MPa/s filling rate do not exceed 358 K. If the system temperature is above 288 K, the maximum temperature at the end of filling may exceed this limit.

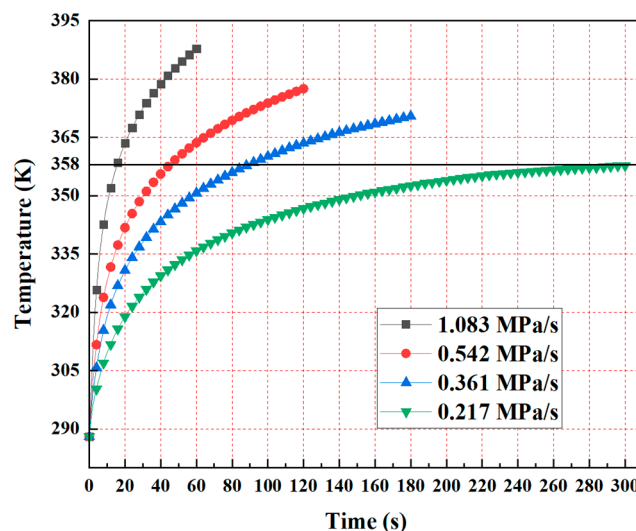


Figure 9. Evolution of the hydrogen temperature rise at different filling rates.

The hydrogen mass flow rates from the different filling rates are shown in Figure 10. The inlet mass flow rate reaches a maximum within the first 10 s. As the hydrogen pressure increases, the inlet mass flow rate decreases non-linearly. When the other filling conditions are the same, the greater hydrogen filling rate, the greater hydrogen mass flow rate of inlet, the greater the velocity of hydrogen inlet, the more turbulent kinetic energy input, the more

internal energy converted from kinetic energy, and the higher the maximum hydrogen temperature rise. However, this inevitably increases the filling time, which cannot meet commercial requirements of completing the filling of on-board hydrogen storage cylinders within 180–300 s.

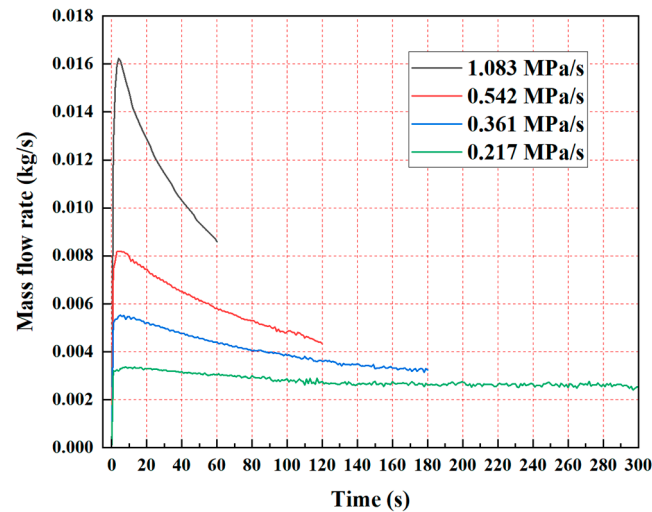


Figure 10. Hydrogen mass flow rates from different filling rates.

### 3.3. Effect of Ambient Temperature

Hydrogen fuel cell vehicles may encounter extreme ambient temperatures when at hydrogen refueling stations. The ambient temperature in winter is often below 258 K, and summer temperatures can reach above 313 K. Different ambient temperatures affect the heat transfer of cylinders. For Cylinder A (24 L), five ambient temperatures of 258, 273, 288, 298, and 313 K are selected, the inlet hydrogen temperature is 253 K, and the other filling parameters are shown as Cases 5–9 in Table 4. The evolutions of the hydrogen temperature rise at different ambient temperatures are shown in Figure 11. As the ambient temperature increases from 258 to 313 K, the hydrogen maximum temperatures are 333, 341, 348, 355, and 363 K, respectively.

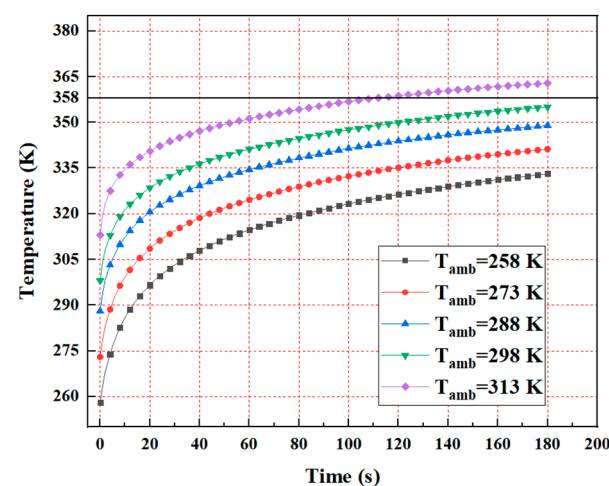
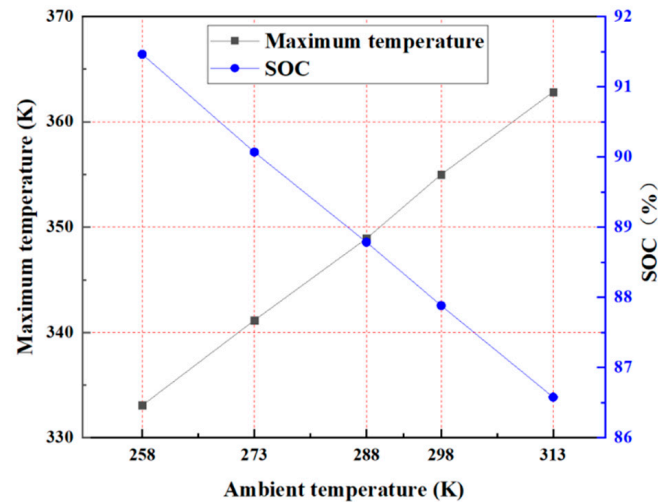


Figure 11. Evolution of the hydrogen temperature rise at different ambient temperatures.

The relationships for the maximum hydrogen temperature and SOC with the ambient temperature at the end of filling are shown in Figure 12. When the other filling parameters are the same, the ambient temperature increases linearly with the maximum hydrogen temperature and decreases linearly with the SOC. When the ambient temperatures are

258 and 273 K, the SOC is greater than 90%. Therefore, when the hydrogen is not pre-cooled or the pre-cooling temperature is high, the hydrogen temperature may exceed 358 K. In addition, if the ambient temperature is high, the SOC cannot reach a full filling state of 90–100%.



**Figure 12.** Relationships for the maximum hydrogen temperature and SOC with the ambient temperature at the end of filling.

### 3.4. Effect of Cylinder Volume

The fast-filling temperature rises of Cylinder A (24 L) and Cylinder B (367 L) are compared and analyzed, and the difference between their length–diameter ratios does not exceed 4.5%. The materials of the two cylinders are the same, the ambient temperature and hydrogen inlet temperature are both 288 K, and the total filling time is 180 s. The other filling parameters are shown as Cases 10 and 11 in Table 4. The evolutions of the hydrogen temperature rise for different cylinder volumes are shown in Figure 13. The maximum hydrogen temperature of Cylinder B (367 L) is 26 K higher than that of Cylinder A (24 L) at the end of filling. Although the larger volume increases the heat transfer surface area between the hydrogen and wall, the ratio of the volume to the heat transfer area increases, and the heat storage capacity of the cylinders is enhanced. Under the same filling conditions, the type IV hydrogen storage cylinders with a capacity of 367 L are prone to overheating during filling; thus, their temperature control strategies are more stringent.

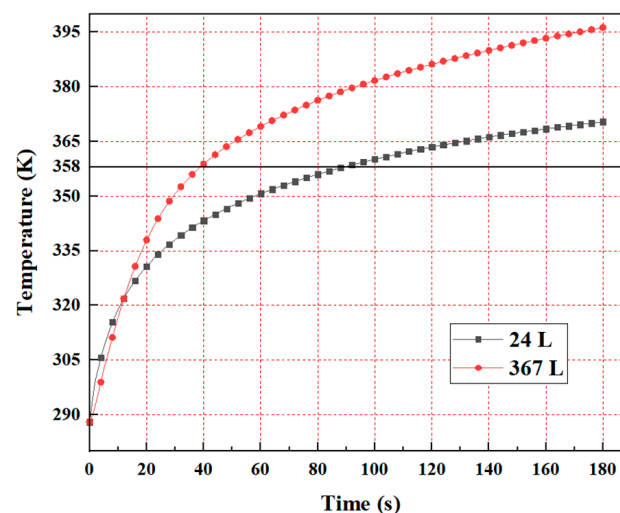


**Figure 13.** Evolution of the hydrogen temperature rise for different cylinder volumes.

### 3.5. Effect of Hydrogen Inlet Temperature

Pre-cooling the inlet hydrogen is an effective way to reduce the temperature rise of hydrogen storage cylinders during fast charging. For Cylinder A (24 L) and Cylinder B (367 L), five different hydrogen inlet temperatures of 233, 253, 263, 273, and 288 K are chosen, while the filling time is 180 s, and other filling parameters are shown as Cases 12–21 in Table 4. The evolutions of the hydrogen temperature rise for Cylinder A at different inlet temperatures are shown in Figure 14a. As the inlet temperature increases from 233 to 288 K, the maximum hydrogen temperature gradually increases. When the inlet temperatures are 273 and 288 K, the maximum hydrogen temperature rise exceeds 358 K. The evolutions of the hydrogen temperature rise for Cylinder B at different inlet temperatures are shown in Figure 14b. The hydrogen temperature rise increases with the hydrogen inlet temperature. Compared with Cylinder A, only when the pre-cooling inlet temperature is 233 K does the maximum hydrogen temperature rise not exceed 358 K.

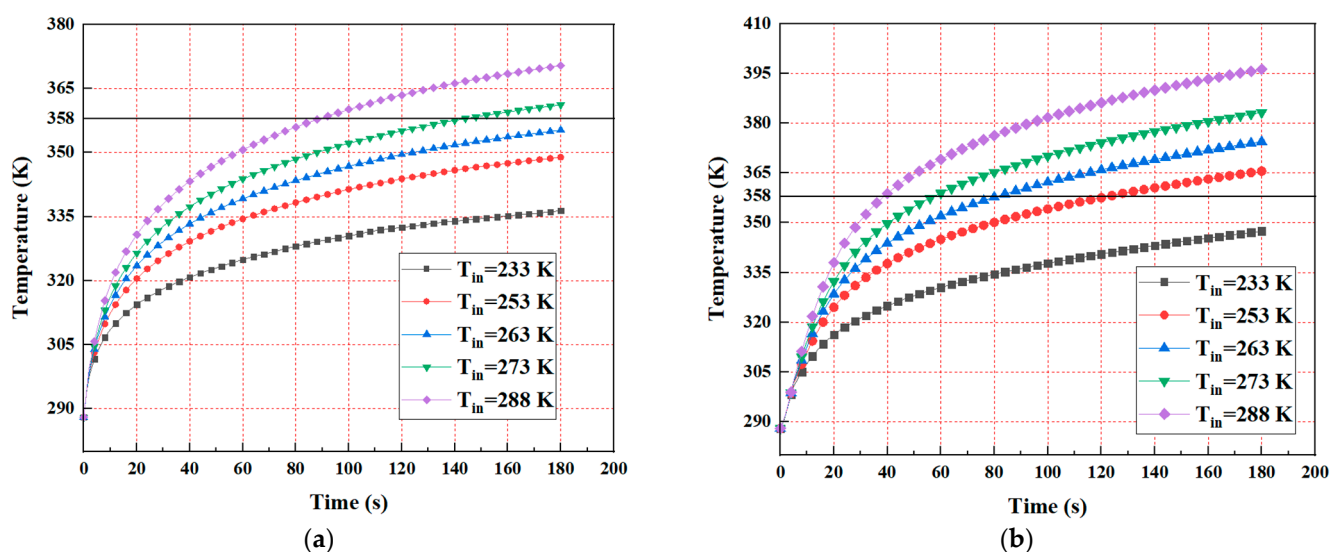


**Figure 14.** Evolutions of the hydrogen temperature rise for (a) Cylinder A and (b) Cylinder B at different inlet temperatures.

The relationships of the maximum hydrogen temperature and SOC with the inlet temperature at the end of filling are shown in Figure 15. The hydrogen inlet temperature increases linearly with the maximum hydrogen temperature and decreases linearly with the SOC. A higher hydrogen inlet temperature causes a lower gas density and SOC for cylinders at the same end pressure. Therefore, a lower inlet hydrogen temperature helps reduce the temperature rise during filling and reduces the time to reach 100% SOC under the same conditions. A larger cylinder volume decreases the required pre-cooling hydrogen temperature. However, the lower pre-cooling hydrogen temperature increases the cooling energy consumption of the refueling station and increases the overall energy costs.

### 3.6. Analysis of Filling Strategies for Large-Volume 70 MPa Type IV Hydrogen Storage Cylinders

Section 3.4 indicates that the hydrogen temperature rise for large-volume type IV hydrogen storage cylinders is greater during filling. Here, the effects of the inlet pressure rise and pre-cooling patterns on the temperature rise of large-volume type IV hydrogen storage cylinders are analyzed, and the optimal filling strategy is determined. Six inlet pressure rise patterns from the cylinders are shown in Figure 16. For Cylinder B (24 L), the inlet hydrogen temperature is 233 K, and the other filling parameters are shown as Cases P1–P6 in Table 4. The six inlet pressure rise patterns are: linear pressure rise (Case P1), fast then slow linear pressure rise (Case P2), slow then fast linear pressure rise (Case P3),

pressure-holding once for 60 s (Case P4), pressure-holding twice for 30 s (Case P5), and pressure-holding thrice for 20 s (Case P6).

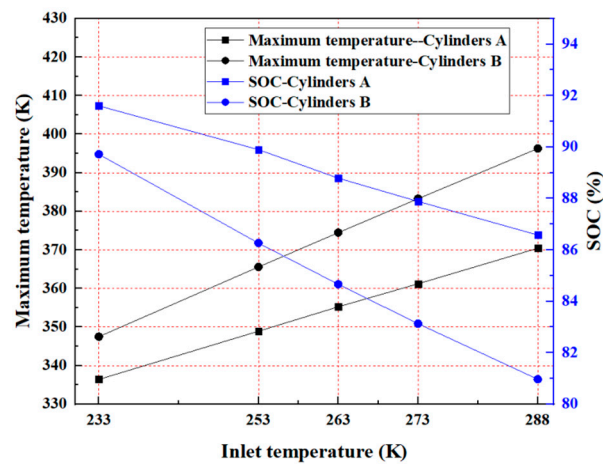


**Figure 15.** Relationships for the maximum hydrogen temperature and SOC with the inlet temperature at the end of filling.

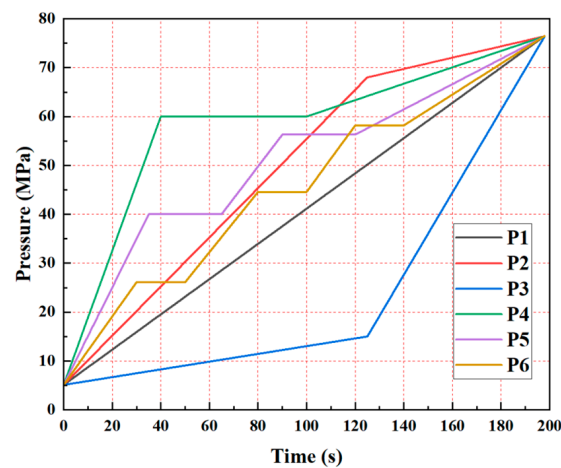


**Figure 16.** Six inlet pressure rise patterns for the cylinders.

The evolutions of the hydrogen temperature rise for Cylinder B at different pressure rise patterns are shown in Figure 17. The temperature rise of the large-volume type IV hydrogen storage cylinders is related to the pressure rise patterns. The maximum temperature rise for Case P3 is the greatest as it reaches 352 K, while the differences for all other patterns are smaller between 348 K and 349 K. Due to the small difference in the maximum temperature at the end of filling, the SOC of the cylinder is between 94.5% and 95.2%. The temperature rise rate in each pattern increases with the pressure rise rate. This is consistent with fast-filling tests under different pressure rise patterns by Hirofani et al. [27] for 65-L type IV hydrogen storage cylinders.

When the total filling time is 198 s and the total pressure-holding time is 60 s, the maximum temperature rises for Cases P4, P5, and P6 (different pressure-holding times) differ little compared with the linear pressure rise pattern. However, a greater pressure rise rate may cause the cylinder to exceed 358 K before being filled, which will require the hydrogenation machine to have a greater flow rate. When the total filling time is 198 s, the pre-cooling hydrogen temperature is 233 K, and the ambient temperature is 288 K. Then, the maximum temperature of Cylinder B does not exceed 358 K under the different pressure rise patterns. However, if the ambient temperature is high, the hydrogen temperature rise may exceed 358 K with a large pressure rise rate. Therefore, if the total filling time

is determined, a high pressure rise rate should be avoided during filling, and the linear pressure rise pattern is optimal.

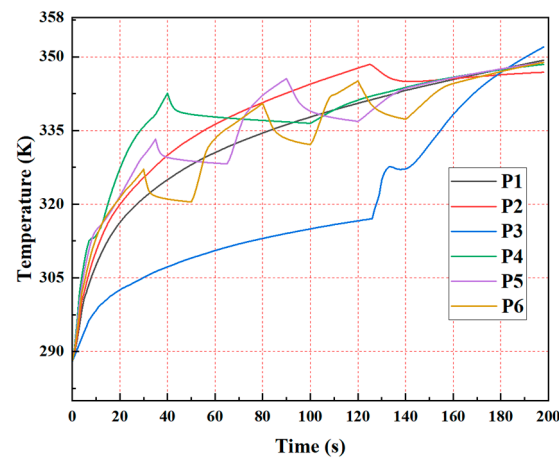


**Figure 17.** Evolutions of the hydrogen temperature rise for Cylinder B at different pressure rise patterns.

Section 3.5 indicates that when the hydrogen pre-cooling temperature of Cylinder B is 233 K, the maximum hydrogen temperature does not exceed 358 K. The lower pre-cooling hydrogen temperature causes a greater cooling energy consumption at the hydrogen refueling station and increases the overall energy cost. Without considering any losses, the theoretical cooling energy of the heat exchanger is equal to the product of the difference in enthalpy of the gas that passes through the heat exchanger and the mass flow rate [34]. As shown in Figure 10, the inlet mass flow rate at the initial filling stage is relatively high and gradually decreases during filling. Therefore, the cooling energy required at the initial stage is greater than at latter stages, and reducing the initial cooling energy is key to optimizing the pre-cooling filling strategy. Four pre-cooling patterns for the cylinders are shown in Figure 18. These are given as follows. Case T1: first 30 s at 263 K, then 233 K; Case T2: first 30 s at 273 K, then 233 K; Case T3: first 30 s at 288 K, then 233 K; and Case T4: first 50 s at 263 K, then 233 K. The other filling parameters are shown as Cases T1–T4 in Table 4.

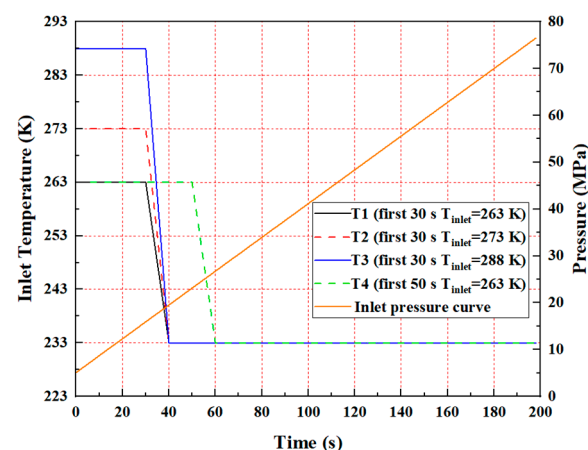


**Figure 18.** Four pre-cooling patterns from the cylinders.

In Figure 19, the increased pre-cooling temperature at the initial filling stage causes the highest temperature rise for Cases T1–T4 to be higher than the 233 K pre-cooling temperature over the entire process, and the maximum hydrogen temperatures for Cases T3 and T4 exceed 358 K. The hydrogen density, SOC, and maximum temperature data under different pre-cooling patterns are shown in Table 5. Compared with the entire

pre-cooling process of 233 K, the SOC for Cases T1–T4 at the end of filling decreased by 1–2%. The maximum temperatures of Cases T1 and T2 do not exceed the limit, but Case T2 consumes less cooling energy. Therefore, it is appropriate to adopt the Case T2 pre-cooling strategy for large-volume cylinders. If the ambient temperature is above 288 K, the initial hydrogen inlet temperature and pre-cooling time of 233 K need to be reset to avoid exceeding the limit.

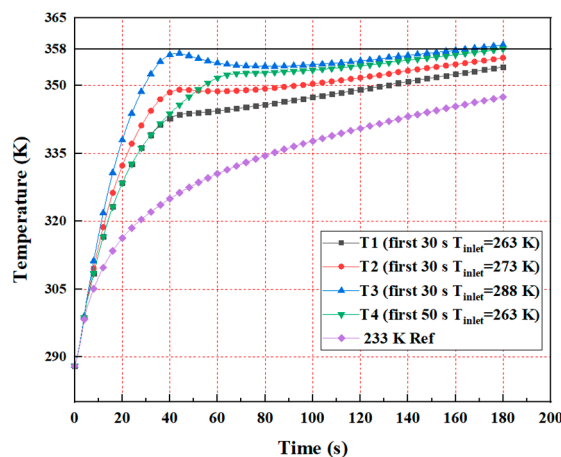


**Figure 19.** Evolutions of the hydrogen temperature rise of Cylinder B at different pre-cooling patterns.

**Table 5.** Hydrogen density, SOC, and maximum temperature under different pre-cooling patterns.

	233 K $T_{ref}$	Case T1	Case T2	Case T3	Case T4
Density/kg·m <sup>-3</sup>	38.25	37.82	37.69	37.51	37.5
SOC/%	95.15	94.08	93.76	93.31	93.28
Max temperature/K	349	355	357	361	359.5

#### 4. Conclusions and Suggestions

- (1) The temperature distributions of hydrogen inside the cylinders are uneven, and the maximum hydrogen temperature during the filling process is near the cylinder tails. The temperature distributions of the plastic liner and CFRP layer are relatively uniform, and the maximum temperature is much lower than the hydrogen temperature in the cylinders. At greater distances from the inlet in the axial direction, the hydrogen temperature increases. Therefore, it is recommended that the temperature sensor probe on the valve be placed in the inlet area away from the jet influence zone.
- (2) A greater hydrogen filling rate causes a shorter filling time and a larger hydrogen temperature rise at the end of filling. A smaller hydrogen filling rate helps reduce the temperature rise of the cylinders, but this also increases the filling time. The ambient temperature has an increasing linear relationship with the maximum hydrogen temperature and a decreasing linear relationship with the SOC. When the hydrogen is not pre-cooled or the pre-cooling temperature is high, high ambient temperatures may cause the hydrogen temperature to exceed 358 K.
- (3) The fast-filling temperature rise of Cylinder A (24 L) and Cylinder B (367 L) are compared and analyzed, the maximum hydrogen temperature of Cylinder B (367 L) is 26 K higher than that of Cylinder A (24 L) at the end of filling, the type IV hydrogen storage cylinders with a capacity of 367 L are prone to overheating during filling, so their temperature control strategies are more stringent. The hydrogen inlet temperature has an increasing linear relationship with the maximum hydrogen temperature and a decreasing linear relationship with the SOC. When the pre-cooling temperature is greater than or equal to 273 K, the maximum temperature rises of the 24 L cylinder in the 180 s fast-filling process exceeds 358 K. The maximum temperature rise of the

367 L cylinder does not exceed 358 K when the pre-cooling temperature is 233 K. By reducing the inlet hydrogen temperature, the temperature rise of the cylinders during fast filling can be effectively controlled, and a larger gas cylinder volume gives a smaller required pre-cooling hydrogen temperature.

- (4) The maximum hydrogen temperature of the slow then the fast linear pressure rise pattern is the greatest, and the differences from the other patterns are small. The temperature rise rate in each pattern increases with the pressure rise rate. When the total filling time is 198 s, the pre-cooling hydrogen temperature is 233 K, and the ambient temperature is 288 K. The maximum temperature of the large-volume cylinders does not exceed 358 K in the considered pressure rise patterns. However, for high ambient temperatures, the hydrogen temperature rise may exceed 358 K in patterns with large pressure rise rates. Therefore, if the total filling time is determined, high pressure rise rates should be avoided during filling, and a linear pressure rise pattern is optimal.
- (5) A lower pre-cooling hydrogen temperature increases the cooling energy consumption of the hydrogen refueling station and increases the overall energy costs. The cooling energy required at the initial filling stage is greater than the latter stages, and reducing the initial cooling energy is key to optimizing the pre-cooling filling strategy. The “first 30 s at 273 K, then 233 K” pre-cooling strategy is best for large-volume cylinders. If the ambient temperature is above 288 K, the initial hydrogen inlet temperature and pre-cooling time of 233 K need to be reset to avoid exceeding the limits.
- (6) It is suggested that temperature rise rules and temperature rise control strategies of 70 MPa Type IV hydrogen storage cylinders for hydrogen fuel cells in heavy-duty trucks with a volume larger than 450 L and on-board hydrogen storage cylinder sets during the filling process be further studied.

**Author Contributions:** Conceptualization, J.L. (Jiepu Li) and J.L. (Junhao Liu); methodology, X.L.; formal analysis, J.L. (Jiepu Li) and B.Z.; investigation, B.Z., D.W., and J.L. (Jiepu Li); data curation, S.G.; writing—original draft preparation, J.L. (Jiepu Li); writing—review and editing, J.L. (Junhao Liu); supervision, X.L.; project administration, J.S. All authors have read and agreed to the published version of the manuscript.

**Funding:** This research was funded by the National Key Research and Development Program of China: 2019YFB1504805; Science and Technology Program of China State Administration for Market Regulation: 2022MK203; Science and Technology Program of CSEI: 2021youth18.

**Data Availability Statement:** Not applicable.

**Conflicts of Interest:** The authors declare no conflict of interest.

## Nomenclature

### Symbols

$E$	Total energy of the gas (J/kg)
$G_k$	Generation of turbulence kinetic energy
$h$	Specific enthalpy of hydrogen (kJ/kg)
$k$	Turbulence kinetic energy ( $\text{m}^2/\text{s}^2$ )
$k_{eff}$	Effective thermal conductivity (W/m·K)
$M_t$	Turbulent Mach number
$p$	Absolute pressure (MPa)
$r$	Radial distance (m)
$t$	Time (s)
$u$	Axial velocity (m/s)
$D_i$	Diameter (mm)
$L$	Length (mm)
$m$	Maximum storage quality (kg)
$D_{in}$	Inlet diameter (mm)

$T_1$	Plastic liner thickness (mm)
$T_2$	CFRP layer thickness (mm)
$T$	Temperature
$v$	Radial velocity (m/s)
$x$	Axial distance (m)
$Y_M$	Fluctuating dilatation in compressible turbulence
Greek Letters	
$\varepsilon$	Turbulence dissipation rate ( $\text{m}^2/\text{s}^3$ )
$\eta$	Efficiency
$\rho$	Density ( $\text{kg}/\text{m}^3$ )
$\mu$	Dynamic viscosity ( $\text{N}\cdot\text{s}/\text{m}^2$ )
$\mu_t$	Turbulence viscosity
Subscripts	
t	Turbulent
eff	Effective
wall	Wall temperature
in	Inlet of gas
gas	Gas in the cylinder
amb	Ambient
inlet	Inlet pre-cooling hydrogen
i	Inner
ref	Reference

## References

- Bakker, S.; van Lente, H.; Meeus, M.T. Credible expectations—The US Department of Energy’s Hydrogen Program as enactor and selector of hydrogen technologies. *Technol. Forecast. Soc. Chang.* **2012**, *79*, 1059–1071. [[CrossRef](#)]
- Matsuo, Y.; Endo, S.; Nagatomi, Y.; Shibata, Y.; Komiyama, R.; Fujii, Y. A quantitative analysis of Japan’s optimal power generation mix in 2050 and the role of CO<sub>2</sub>-free hydrogen. *Energy* **2018**, *165*, 1200–1219. [[CrossRef](#)]
- Sgobbi, A.; Nijis, W.; De Miglio, R.; Chiodi, A.; Gargiulo, M.; Thiel, C. How far away is hydrogen? Its role in the medium and long-term decarbonisation of the European energy system. *Int. J. Hydrogen Energy* **2016**, *41*, 19–35. [[CrossRef](#)]
- Jain, I. Hydrogen the fuel for 21st century. *Int. J. Hydrogen Energy* **2009**, *34*, 7368–7378. [[CrossRef](#)]
- Niaz, S.; Manzoor, T.; Pandith, A.H. Hydrogen storage: Materials, methods and perspectives. *Renew. Sustain. Energy Rev.* **2015**, *50*, 457–469. [[CrossRef](#)]
- Zheng, J.; Liu, Z.; Hua, Z.; Guch, W.G.; Chen, L. Research status-in-situ and key challenges in hydrogen safety. *J. Saf. Environ.* **2020**, *20*, 106–115. [[CrossRef](#)]
- Manoharan, Y.; Hosseini, S.E.; Butler, B.; Alzahrani, H.; Senior, B.T.F.; Ashuri, T.; Krohn, J. Hydrogen fuel cell vehicles; current status and future prospect. *Appl. Sci.* **2019**, *9*, 2296. [[CrossRef](#)]
- Bustamante Valencia, L.; Blanc-Vannet, P.; Domergue, D.; Heudier, L.; Jamois, D. Thermal history resulting in the failure of lightweight fully-wrapped composite pressure vessel for hydrogen in a fire experimental facility. *Fire Technol.* **2016**, *52*, 421–442. [[CrossRef](#)]
- Zhang, M.; Lv, H.; Kang, H.; Zhou, W.; Zhang, C. A literature review of failure prediction and analysis methods for composite high-pressure hydrogen storage tanks. *Int. J. Hydrogen Energy* **2019**, *44*, 25777–25799. [[CrossRef](#)]
- Ahluwalia, R.K.; Hua, T.; Peng, J. On-board and Off-board performance of hydrogen storage options for light-duty vehicles. *Int. J. Hydrogen Energy* **2012**, *37*, 2891–2910. [[CrossRef](#)]
- Pépin, J.; Lainé, E.; Grandidier, J.-C.; Benoit, G.; Mellier, D.; Weber, M.; Langlois, C. Replication of liner collapse phenomenon observed in hyperbaric type IV hydrogen storage vessel by explosive decompression experiments. *Int. J. Hydrogen Energy* **2018**, *43*, 4671–4680. [[CrossRef](#)]
- Sun, Y.; Lv, H.; Zhou, W.; Zhang, C. Research on hydrogen permeability of polyamide 6 as the liner material for type IV hydrogen storage tank. *Int. J. Hydrogen Energy* **2020**, *45*, 24980–24990. [[CrossRef](#)]
- Yersak, T.A.; Baker, D.R.; Yanagisawa, Y.; Slavik, S.; Immel, R.; Mack-Gardner, A.; Herrmann, M.; Cai, M. Predictive model for depressurization-induced blistering of type IV tank liners for hydrogen storage. *Int. J. Hydrogen Energy* **2017**, *42*, 28910–28917. [[CrossRef](#)]
- Durbin, D.; Malardier-Jugroot, C. Review of hydrogen storage techniques for on board vehicle applications. *Int. J. Hydrogen Energy* **2013**, *38*, 14595–14617. [[CrossRef](#)]
- Maus, S.; Hapke, J.; Ranong, C.N.; Wüchner, E.; Friedlmeier, G.; Wenger, D. Filling procedure for vehicles with compressed hydrogen tanks. *Int. J. Hydrogen Energy* **2008**, *33*, 4612–4621. [[CrossRef](#)]
- Yang, J.C. A thermodynamic analysis of refueling of a hydrogen tank. *Int. J. Hydrogen Energy* **2009**, *34*, 6712–6721. [[CrossRef](#)]
- Zhang, J.; Fisher, T.S.; Ramachandran, P.V.; Gore, J.P.; Mudawar, I. A review of heat transfer issues in hydrogen storage technologies. *J. Heat Transfer.* **2005**, *127*, 1391–1399. [[CrossRef](#)]

18. Zhao, Y.; Liu, G.; Liu, Y.; Zheng, J.; Chen, Y.; Zhao, L.; Guo, J.; He, Y. Numerical study on fast filling of 70 MPa type III cylinder for hydrogen vehicle. *Int. J. Hydrogen Energy* **2012**, *37*, 17517–17522. [[CrossRef](#)]
19. Sapre, S.; Pareek, K.; Rohan, R.; Singh, P.K. H<sub>2</sub> refueling assessment of composite storage tank for fuel cell vehicle. *Int. J. Hydrogen Energy* **2019**, *44*, 23699–23707. [[CrossRef](#)]
20. Xiao, J.; Wang, X.; Bénard, P.; Chahine, R. Determining hydrogen pre-cooling temperature from refueling parameters. *Int. J. Hydrogen Energy* **2016**, *41*, 16316–16321. [[CrossRef](#)]
21. Schneider, J.; Meadows, G.; Mathison, S.R.; Veenstra, M.J.; Shim, J.; Immel, R.; Wistoft-Ibsen, M.; Quong, S.; Greisel, M.; McGuire, T. Validation and sensitivity studies for SAE J2601, the light duty vehicle hydrogen fueling standard. *SAE Int. J. Altern. Powertrains* **2014**, *3*, 257–309. [[CrossRef](#)]
22. Li, J.-Q.; Myoung, N.-S.; Kwon, J.-T.; Jang, S.-J.; Lee, T. A study on the prediction of the temperature and mass of hydrogen gas inside a tank during fast filling process. *Energies* **2020**, *13*, 6428. [[CrossRef](#)]
23. Li, J.-Q.; Myoung, N.-S.; Kwon, J.-T.; Jang, S.-J.; Lee, T.; Lee, Y.-H. A theoretical analysis of temperature rise of hydrogen in high-pressure storage cylinder during fast filling process. *Adv. Mech. Eng.* **2020**, *12*, 1687814020971920. [[CrossRef](#)]
24. Xue, L.; Deng, J.; Wang, X.; Wang, Z.; Liu, B. Numerical Simulation and Optimization of Rapid Filling of High-Pressure Hydrogen Storage Cylinder. *Energies* **2022**, *15*, 5189. [[CrossRef](#)]
25. Liu, Y.-L.; Zhao, Y.-Z.; Zhao, L.; Li, X.; Chen, H.-g.; Zhang, L.-F.; Zhao, H.; Sheng, R.-H.; Xie, T.; Hu, D.-H. Experimental studies on temperature rise within a hydrogen cylinder during refueling. *Int. J. Hydrogen Energy* **2010**, *35*, 2627–2632. [[CrossRef](#)]
26. Zhao, L.; Liu, Y.; Yang, J.; Zhao, Y.; Zheng, J.; Bie, H.; Liu, X. Numerical simulation of temperature rise within hydrogen vehicle cylinder during refueling. *Int. J. Hydrogen Energy* **2010**, *35*, 8092–8100. [[CrossRef](#)]
27. Hirotani, R.; Tomioka, J.; Maeda, Y.; Mitsuishi, H.; Watanabe, S. *Thermal Behavior in Hydrogen Storage Tank for Fuel Cell Vehicle on Fast Filling*; Society of Automotive Engineers Technical Report; SAE International: Warrendale, PA, USA, 2007. [[CrossRef](#)]
28. Zhao, B.; Wei, H.; Peng, X.; Feng, J.; Jia, X. Experimental and Numerical Research on Temperature Evolution during the Fast-Filling Process of a Type III Hydrogen Tank. *Energies* **2022**, *15*, 3811. [[CrossRef](#)]
29. Liu, J.; Ma, H.; Zheng, S.; Zhang, Z.; Zheng, J.; Zhao, Y. Numerical investigation on temperature-rise of on-bus gaseous hydrogen storage cylinder with different thickness of liner and wrapping material. *Int. J. Hydrogen Energy* **2021**, *46*, 20607–20620. [[CrossRef](#)]
30. Acosta, B.; Moretto, P.; de Miguel, N.; Ortiz, R.; Harskamp, F.; Bonato, C. JRC reference data from experiments of on-board hydrogen tanks fast filling. *Int. J. Hydrogen Energy* **2014**, *39*, 20531–20537. [[CrossRef](#)]
31. Galassi, M.C.; Baraldi, D.; Iborra, B.A.; Moretto, P. CFD analysis of fast filling scenarios for 70 MPa hydrogen type IV tanks. *Int. J. Hydrogen Energy* **2012**, *37*, 6886–6892. [[CrossRef](#)]
32. Deng, S.; Xiao, J.; Bénard, P.; Chahine, R. Determining correlations between final hydrogen temperature and refueling parameters from experimental and numerical data. *Int. J. Hydrogen Energy* **2020**, *45*, 20525–20534. [[CrossRef](#)]
33. Xiao, J.; Cheng, J.; Wang, X.; Bénard, P.; Chahine, R. Final hydrogen temperature and mass estimated from refueling parameters. *Int. J. Hydrogen Energy* **2018**, *43*, 22409–22418. [[CrossRef](#)]
34. Melideo, D.; Baraldi, D. CFD analysis of fast filling strategies for hydrogen tanks and their effects on key-parameters. *Int. J. Hydrogen Energy* **2015**, *40*, 735–745. [[CrossRef](#)]
35. Ramasamy, V.; Richardson, E. Thermal response of high-aspect-ratio hydrogen cylinders undergoing fast-filling. *Int. J. Heat Mass Transf.* **2020**, *160*, 120179. [[CrossRef](#)]
36. Wu, X.; Liu, J.; Shao, J.; Deng, G. Fast filling strategy of type III on-board hydrogen tank based on time-delayed method. *Int. J. Hydrogen Energy* **2021**, *46*, 29288–29296. [[CrossRef](#)]
37. Melideo, D.; Baraldi, D.; Galassi, M.C.; Cebolla, R.O.; Iborra, B.A.; Moretto, P. CFD model performance benchmark of fast filling simulations of hydrogen tanks with pre-cooling. *Int. J. Hydrogen Energy* **2014**, *39*, 4389–4395. [[CrossRef](#)]
38. Li, Q.; Zhou, J.; Chang, Q.; Xing, W. Effects of geometry and inconstant mass flow rate on temperatures within a pressurized hydrogen cylinder during refueling. *Int. J. Hydrogen Energy* **2012**, *37*, 6043–6052. [[CrossRef](#)]
39. Dicken, C.; Mérida, W. Modeling the transient temperature distribution within a hydrogen cylinder during refueling. *Numer. Heat Transf. Part A Appl.* **2007**, *53*, 685–708. [[CrossRef](#)]
40. Bourgeois, T.; Ammouri, F.; Weber, M.; Knapik, C. Evaluating the temperature inside a tank during a filling with highly-pressurized gas. *Int. J. Hydrogen Energy* **2015**, *40*, 11748–11755. [[CrossRef](#)]
41. Kim, M.-S.; Jeon, H.-K.; Lee, K.-W.; Ryu, J.-H.; Choi, S.-W. Analysis of Hydrogen Filling of 175 Liter Tank for Large-Sized Hydrogen Vehicle. *Appl. Sci.* **2022**, *12*, 4856. [[CrossRef](#)]
42. Suryan, A.; Kim, H.D.; Setoguchi, T. Three dimensional numerical computations on the fast filling of a hydrogen tank under different conditions. *Int. J. Hydrogen Energy* **2012**, *37*, 7600–7611. [[CrossRef](#)]
43. Suryan, A.; Kim, H.D.; Setoguchi, T. Comparative study of turbulence models performance for refueling of compressed hydrogen tanks. *Int. J. Hydrogen Energy* **2013**, *38*, 9562–9569. [[CrossRef](#)]
44. Sommer, T.; So, R.; Zhang, H. Near-wall variable-Prandtl-number turbulence model for compressible flows. *AIAA J.* **1993**, *31*, 27–35. [[CrossRef](#)]
45. Dicken, C.; Merida, W. Measured effects of filling time and initial mass on the temperature distribution within a hydrogen cylinder during refuelling. *J. Power Sources* **2007**, *165*, 324–336. [[CrossRef](#)]

46. Liu, J.; Zheng, S.; Zhang, Z.; Zheng, J.; Zhao, Y. Numerical study on the fast filling of on-bus gaseous hydrogen storage cylinder. *Int. J. Hydrogen Energy* **2020**, *45*, 9241–9251. [[CrossRef](#)]
47. Oh, S.J.; Yoon, J.H.; Jeon, K.S.; Choi, J. A numerical study on characteristics of heat transfer in hydrogen filling storage vessel by charging conditions. *Int. J. Hydrogen Energy* **2022**, *47*, 25679–25695. [[CrossRef](#)]

**Disclaimer/Publisher’s Note:** The statements, opinions and data contained in all publications are solely those of the individual author(s) and contributor(s) and not of MDPI and/or the editor(s). MDPI and/or the editor(s) disclaim responsibility for any injury to people or property resulting from any ideas, methods, instructions or products referred to in the content.